Frequency modulated (FM) time delay photoacoustic and photothermal wave spectroscopies. Technique, instrumentation, and detection. Part III: Mirage effect spectrometer, dynamic range, and comparison to pseudo-random-binary-sequence (PRBS) method

Andreas Mandelis and Linda L. M. Borm

Photoacoustic and Photothermal Sciences Laboratory, Department of Mechanical Engineering, University of Toronto, Toronto, Ontario M5S 1A4, Canada

John Tiessinga

Research Laboratory, West Tower, Ministry of Transportation and Communications, Downsview, Ontario M3M 1J8, Canada

(Received 14 October 1985; accepted for publication 8 November 1985)

A detailed comparison is presented between the time delay and the pseudo-random-binary-sequence (PRBS) methods of excitation and mirage effect response. Both time delay domain dynamic system response and frequency domain spectral functions were calculated via FFT methods. The results show that the FM time delay spectrometer exhibits superior performance to the PRBS device and is optimally suitable for nondestructive and depth-profiling studies. The detailed examination of, and comparison between, the time delay and spectral dynamic functions of our FM time delay photothermal wave spectrometer and those of a PRBS-driven device has proven that the former apparatus is capable of producing superior quality time delay and spectral function information when tested on a fast, flat frequency response mirage effect system. The FM time delay photoacoustic/photothermal wave technique and instrumentation of this work holds excellent promise for nondestructive evaluation and depth-profiling applications in scientific research as well as industrial development laboratories.

INTRODUCTION

FM time delay photothermal wave spectroscopy has emerged as a powerful technique for the study of Mirage effect related phenomena at material interfaces (this work, Part II). The potential of this technique is more general, however, than the photothermal deflection apparatus presented in Part II might suggest. The most promising features of our system are (i) its ability to perform *fast* measurements of the frequency spectrum of a specimen, a consequence of the FFT nature of data analysis and (ii) the mathematical Dirac delta function thermal pulse equivalent of the specimen response to the exciting cw radiation via the impulse response of the system, a consequence of the nature of sample excitation and correlation analysis of data. Both features have important implications for the suitability of the FM time delay spectrometer for nondestructive evaluation (NDE) and depth profiling studies with simultaneous, rather than sequential, information acquisition from a range of depths in a material. These features, however, are not unique to the time delay domain excitation, but rather commonly shared with more conventional random noise methods.[1,2] Therefore, the choice of the optimal method is a very important consideration, impacting directly on the quality and interpretability of data obtained by a given time delay technique. In this work we have made a detailed comparison of the time delay domain and spectral function quality and dynamic range between our FM time delay photothermal spectrometer/imager and the same apparatus excited by a 127-bit-long PRBS optical pulse.

I. EXPERIMENTAL

The FM time delay spectrometer used in this work has been described in detail elsewhere (Part II of this work, Fig. 1) and was set up for mirage effect phenomena probing via a fast detector unit with a flat frequency response up to ~ 30 MHz. A swept square wave excitation was employed from dc to 1280 Hz with a sweep time of 0.41 s. The PRBS waveform was introduced into the system for comparison with the swept wave by constructing an analog 127-bit-long PRBS voltage generator of variable peak-to-peak amplitude and pseudoperiod. The output of this device was used as the input to an Isomet model # 1201E-2 acousto-optic (A/O) modulator coupled to the Nd^{3+}:YAG pump laser 1.06-μm line of our system. The modulation depth of the A/O modulator was further maximized by adjusting the amplitude of the voltage generator output waveform and the bias adjust of the A/O analog driver. The rest of the system was identical to the one described in Part II. The input and output signals were introduced to channels A and B, respectively, of the Nicolet 660A dual channel FFT analyzer. Signal averaging was performed for both types of excitation methods in this work over 1000 sweeps per 1024-bit sample.

II. PRBS SYSTEM PERFORMANCE

In order to characterize the performance of the PRBS excitation with respect to physical parameters of the mirage effect system, the impulse response $h(\tau)$ and cross correlation $R_{xy}(\tau)$ of the input and output were studied as func-

 0034-6748/86/040630-06$01.30

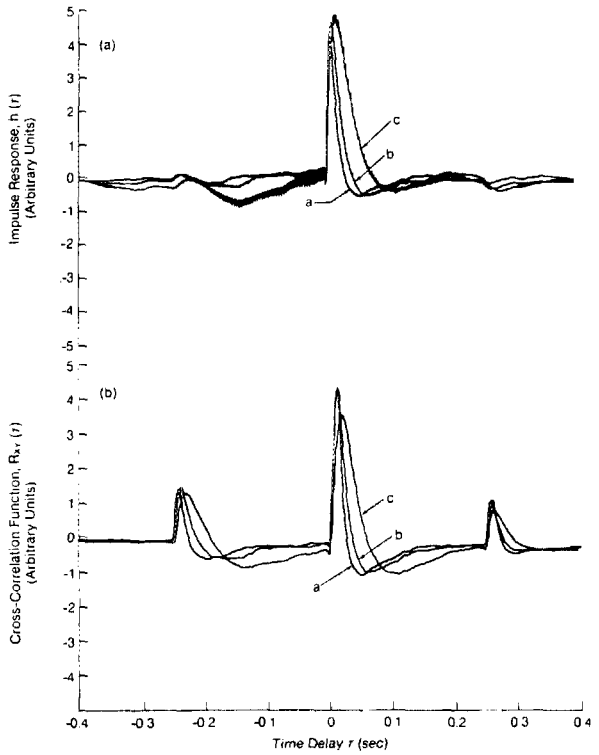

FIG. 1. Water–blackbody interface mirage effect response to PRBS excitation. (a) Impulse response. Curve a: $x_0 = 10\ \mu$m, $\tau_0 = 3.91$ ms, $\tau_{FWHM} = 6.48$ ms, $\tau_{min} = 24.22$ ms; Curve b: $x_0 = 70\ \mu$m, $\tau_0 = 5.08$ ms, $\tau_{FWHM} = 9.18$ ms, $\tau_{min} = 32.03$ ms; Curve c: $x_0 = 130\ \mu$m, $\tau_0 = 7.81$ ms, $\tau_{FWHM} = 16.84$ ms; $\tau_{min} = 56.64$ ms. (b) Cross-correlation function. Curve a: $x_0 = 10\ \mu$m, $\tau_0 = 3.91$ ms, $\tau_{FWHM} = 6.57$ ms, $\tau_{min} = 25.78$ ms, $\tau_2 = 128.91$ ms; Curve b: $x_0 = 70\ \mu$m, $\tau_0 = 4.69$ ms, $\tau_{FWHM} = 9.23$ ms, $\tau_{min} = 30.47$ ms, $\tau_2 = 129.69$ ms; Curve c: $x_0 = 130\ \mu$m, $\tau_0 = 8.59$ ms, $\tau_{FWHM} = 17.34$ ms, $\tau_{min} = 56.64$ ms, $\tau_2 = 132.42$ ms. The various quantities have been defined in the text.

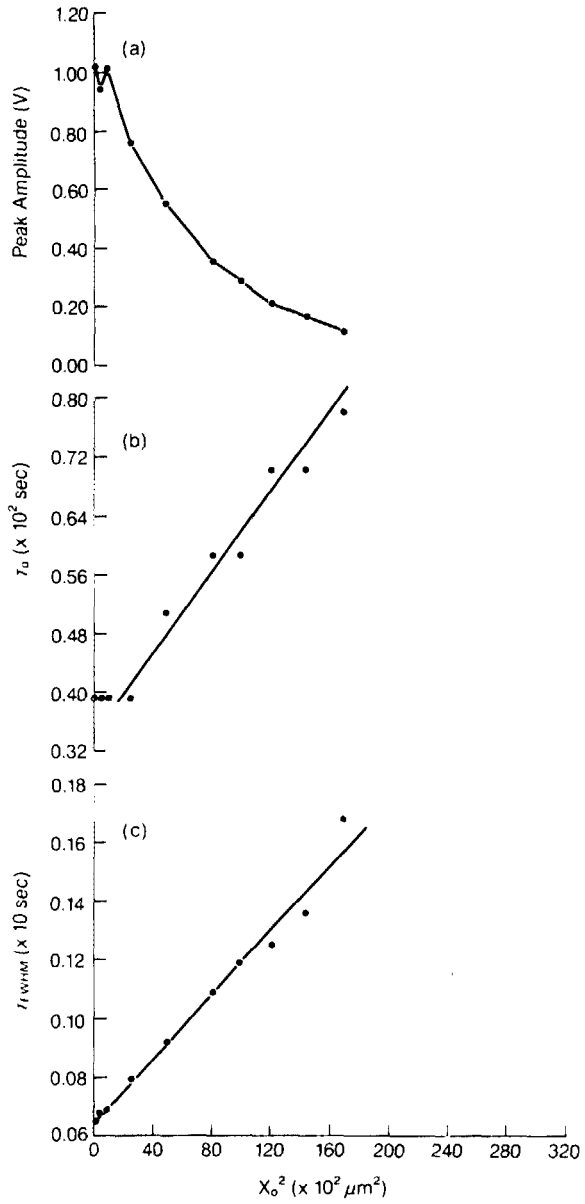

FIG. 2. PRBS spectrometer impulse response parameter dependence on probe beam offset. (a) Magnitude; (b) Peak delay time; (c) Full width at half-maximum time.

tions of the transverse probe beam offset in water above an anodized aluminum blackbody excited by the Nd^{3+}:YAG laser. Figure 1 shows the superposition of three such curves for the impulse response, Fig. 1(a), and the cross-correlation function, Fig. 1(b), with the nominal beam offset as a parameter. In these curves, which were generated on the screen of the FFT analyzer, the various times are defined as follows: τ_0 is the peak delay time, τ_{FWHM} is the time delay width of each line at half-maximum, τ_{min} is the time delay corresponding to the signal minimum past the main peak and, in the case of the cross-correlation function, τ_2 is the peak delay time of the positive secondary maximum. The presence of the secondary maxima on both sides of the main peak of $R_{xy}(\tau)$ is associated with the second pseudoharmonic (i.e., the leakage of a fraction of the basic PRBS waveform energy to higher frequencies corresponding to the second multiple of the fundamental pseudoperiod). Such secondary maxima are characteristic of random noise excitations.[3] With our spectrometer they appear also in the impulse response function with lower magnitude than in the cross-correlation plot. The curves of Fig. 1 show an increase in the peak delay time τ_0 and in τ_{FWHM} with increasing beam offset. The magnitudes are unnormalized, however they exhibit a steady decrease with increasing x_0. The undershoots below the zero of the y axis present in both $h(\tau)$ and $R_{xy}(\tau)$ are thought to be due to a rarefaction of the water pressure increase following the main short compressive pulse,[4] as heat is released into the liquid after absorption of the pump laser energy. Figure 2 shows the behavior of the impulse response magnitude (a), τ_0 (b), and τ_{FWHM} (c), with increasing beam offset for the complete experimental range of x_0. In this figure all curves were plotted vs x_0^2. Both τ_0 and τ_{FWHM} show an approximately linear dependence on x_0^2. It is worthwhile noting that τ_0 is essentially independent of x_0 for nominal beam offsets up to $\sim 50\ \mu$m, whereas τ_{FWHM} is increasing in that range of x_0. The cause of the flat value for τ_0 at small beam offsets is in all likelihood the partial blocking of the focused probe beam ($W_0 \cong 120\ \mu$m) by the sample bulk. The initial nonmonotonic amplitude dependence on x_0^2, Fig. 2(a), is also consistent with the same interpretation of the observed anomaly. The behavior of τ_{FWHM} shows,

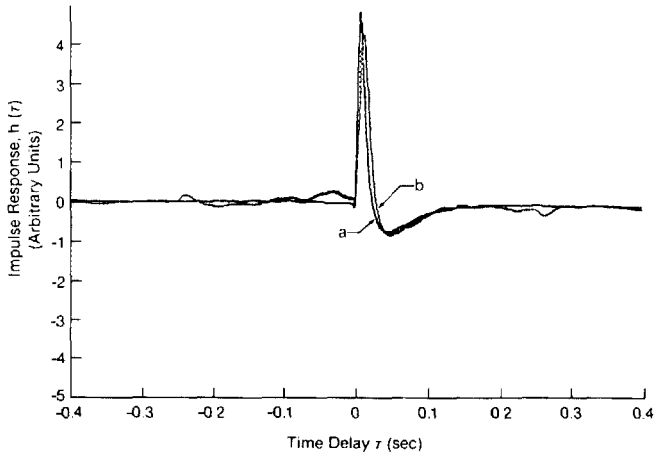

FIG. 3. Comparison of impulse responses between FT time delay (a) and PRBS (b) spectrometers for $x_0 = 10\,\mu$m. (a) $\tau_0 = 2.34$ ms, $\tau_{FWHM} = 5.13$ ms, $\tau_{min} = 23.44$ ms. (b) $\tau_0 = 3.91$ ms, $\tau_{FWHM} = 6.48$ ms, $\tau_{min} = 24.22$ ms.

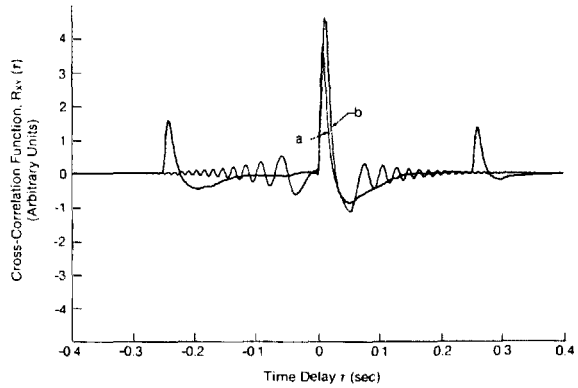

FIG. 4. Comparison of cross-correlation functions between FT time delay (a) and PRBS (b) spectrometers for $x_0 = 10\,\mu$m. (a) $\tau_0 = 2.34$ ms, $\tau_{FWHM} = 5.2$ ms, $\tau_{min} = 26.56$ ms. (b) $\tau_0 = 3.91$ ms, $\tau_{FWHM} = 6.57$ ms, $\tau_{min} = 25.78$ ms.

however, that this parameter is more sensitive to minute changes in x_0 than τ_0. Using results from Part II concerning approximate analytical expressions for τ_0 and τ_{FWHM}, together with the slopes of Figs. 2(b) and 2(c) as determined by least-squares fits, we find

$$\alpha_{H_2O} = 1/6S_1 = 0.7\times10^{-3}\ \text{cm}^2/\text{s} \quad (1)$$

and

$$\alpha_{H_2O} = 1/(4\ln 2)S_2 = 1.33\times10^{-3}\ \text{cm}^2/\text{s}, \quad (2)$$

where $S_1 = \Delta\tau_0/\Delta(x_0^2)$ is the slope of Fig. 2(b), and $S_2 = \Delta\tau_{FWHM}/\Delta(x_0^2)$ is the slope of Fig. 2(c). The values for the thermal diffusivity of water estimated in Eqs. (1) and (2) are within a factor of two from the published value[5] 1.4×10^{-3} cm^2/s. The close approximation to that value effected by the slope of Fig. 3(c) is a further manifestation of the higher sensitivity of τ_{FWHM} to the distance from the absorbing surface than that of τ_0 for our PRBS-excited system. Similar results were obtained from the cross-correlation data, thus supporting a heat diffusion mechanism in the water following the generation of an impulsive type heat source at the blackbody surface according to models presented in Part II. This section, therefore, establishes the ability of the PRBS mirage effect spectrometer to monitor the time development of a Dirac delta type thermal pulse equivalent at the sample/water interface. The PRBS response will now be compared to our FM time delay response, which was shown in Part II to monitor the same physical phenomenon.

III. DYNAMIC RANGE PROPERTIES: FM TIME DELAY AND PRBS SPECTROMETERS

Any differences in the quality of the spectra obtained by the FM time delay and the PRBS methods are not, in general, immediately obvious from the visual study of the impulse response and/or the input–output cross-correlation functions only. Closer scrutiny and other time delay domain and spectral parameters must also be considered in order for a complete picture to emerge. Nevertheless, subtle but important differences can be found in directly comparing $h(\tau)$ and $R_{xy}(\tau)$ using the two methods. Figure 3 shows such a comparison between FM time delay and PRBS impulse responses from the blackbody/water interface at nominal beam offsets of 10 μm. The FM time delay spectrometer response peaks at an earlier delay time than the PRBS device. This important difference is due to the extended dynamic range afforded by the FM time delay technique, compared to the nonflat frequency spectrum of the PRBS sequence, as will be seen below. Variations in the absolute magnitude of the peak delay time due to the total number of PRBS bits involved in the waveform have been previously reported by Sugitani and Uejima.[6] The total number of bits comprising a PRBS sequence determines the degree of approximation of the pseudorandom noise thus generated to a binomial distribution around the zero mean value.[7] Therefore, it also determines the degree of flatness of the power spectrum of the response. In Fig. 3 it can be seen that the values of τ_{FWHM} are in better agreement with each other than those for τ_0. It may, therefore, be argued that the measurement of τ_{FWHM} in a PRBS experiment will give a better estimate of the quantity under investigation than τ_0, primarily due to the relative character of the former (difference between two half-power delay times) compared to the absolute character of the latter. Figure 4 shows the comparison between the cross-correlation functions obtained via the two methods. It can be observed that the extended dynamic range of the FM time delay technique completely wipes out the secondary maxima which flank the main peak of the PRBS signal. Instead, the oscillatory behavior characteristic of "ideal" (i.e., mathematical) cross-correlation functions[3] is exhibited.

Figure 5 shows the autocorrelations $R_{xx}(\tau)$ and $R_{yy}(\tau)$ of inputs and outputs, respectively, of the two techniques. In Fig. 5(b) the secondary peaks of the PRBS input autocorrelation are clearly seen at the onset of the second multiple of the frequency band spanned by the PRBS pseudoperiod. These spikes are also present in the PRBS output autocorrelation, albeit much more broadened and of much lower magnitude. A comparison of $R_{xx}(\tau)$ between Figs. 5(a) and 5(b) shows that the PRBS function is more broadened than the FM time delay function on the time scale of the experi-

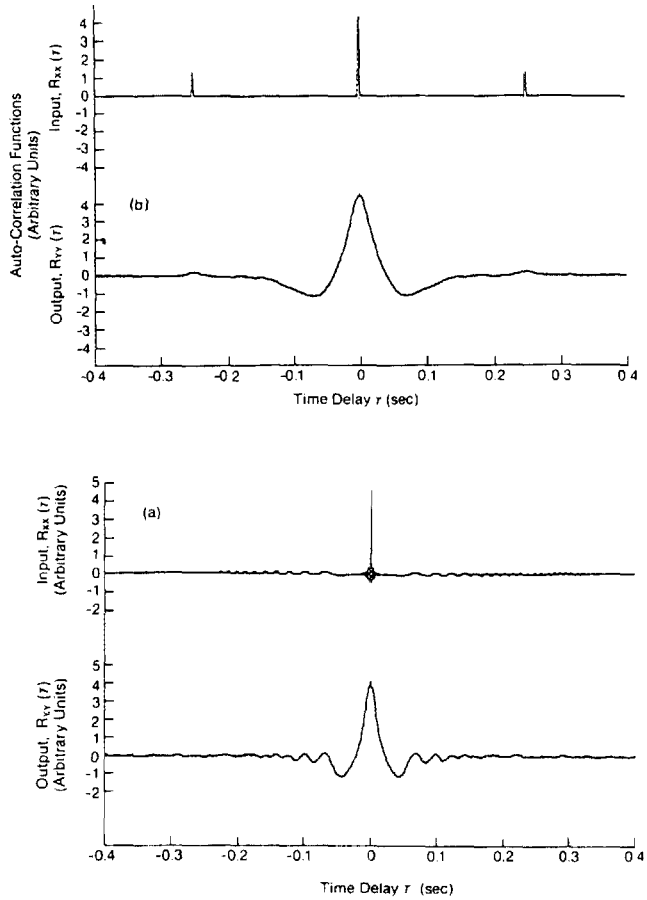

FIG. 5. Autocorrelation functions of system input and output: (a) FT time delay spectrometer; (b) PRBS spectrometer.

ment. Therefore, it is expected that the PRBS $R_{xx}(\tau)$ convolution with the impulse response (i.e., the input/output cross-correlation function, see theorem in Part I) will be somewhat broader than the PRBS impulse response function $h(\tau)$, a fact borne out by our experiments in Fig. 1 upon comparing τ_{FWHM} between the curves of Fig. 1(a) and the corresponding curves of Fig. 1(b). On the other hand, the narrow $R_{xx}(\tau)$ of the FM time delay spectrometer is a closer representation of a Dirac delta function than the PRBS counterpart and produces essentially identical line shapes between $h(\tau)$ and $R_{xy}(\tau)$, as verified in Part II.

Figure 6 compares the one-sided autospectral densities of the two devices between dc and 1 kHz. From this figure two facts become apparent immediately: First, the FM time delay apparatus exhibits a truly flat input $G_{xx}(f)$ up to the highest frequency as expected from the Fourier transform of the Dirac delta function representing the autocorrelation of the input. This is to be compared to the decay of the PRBS spectral contributions to the average power above 200–300 Hz. Second, the uneven distribution in the frequency density of the power input spectrum in the PRBS case results in a steeper decay of its output $G_{yy}(f)$ than the FM time delay signal. This means that the higher frequency components are weighed less in the PRBS experiment, with a concomitant spectral distortion at high frequencies. No indication of even the onset of such a frequency weighing phenomenon is shown by the FM time delay spectrometer within the displayed frequency range. The flatness of the autospectral density function is a further assurance of the mathematical

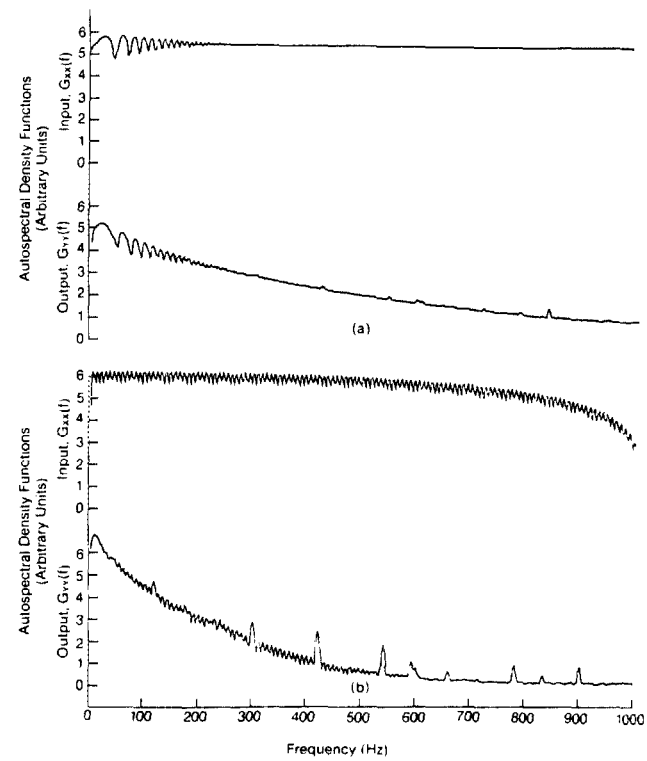

FIG. 6. One-sided autospectral densities of system input and output: (a) FT time delay spectrometer; (b) PRBS spectrometer.

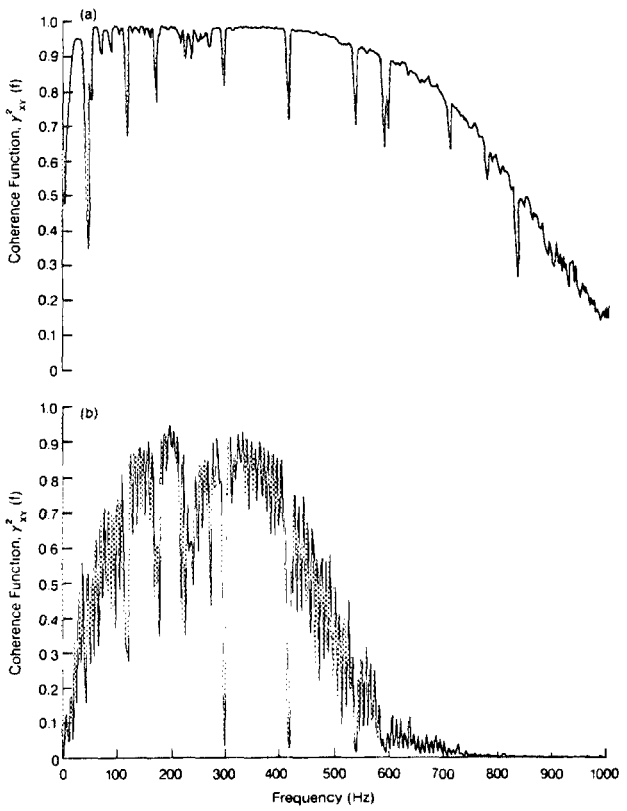

FIG. 7. Coherence functions: (a) FT time delay spectrometer; (b) PRBS spectrometer.

equivalence between the impulse response and cross-correlation functions (see Part I) for the FM time delay spectrometer. Figure 6(b) indicates that this equivalence is not entirely justified for the PRBS spectrometer, due to the autospectral density roll off at high frequencies. It is further apparent from Fig. 6(b) that the autospectral density curve corresponding to PRBS excitation consists of discrete power bands ("sawtoothed response") spanning narrow frequency ranges with a continuous envelope. The corresponding FM time delay curve, on the other hand, is truly continuous aside from a progressively discrete behavior at frequencies below 200 Hz. The discrete power band regions in both Figs. 6(a) and 6(b) are seen to generate similar behavior of the output autospectral densities. This results in a sawtoothed output autospectral density $G_{yy}(f)$ for PRBS excitation, with a continuous envelope throughout much of the spectrum and is directly responsible for the lower quality of the PRBS signal.

Figure 7 is a comparison between the coherence functions obtained from the signal inputs and outputs for the two techniques. The coherence function is a most sensitive indicator of the quality of the relation between input and output. The superior performance of the FM time delay spectrometer is unequivocally exemplified in this figure. Essentially no correlation can be found above 600 Hz for the PRBS method, while a strong relation between input and output well beyond 1 kHz is observed for the FM time delay system. The dips in the coherence functions are due to nonsystem related signal sources, such as line ripple and multiples of 60 Hz. These sources are completely deterministic at well-defined frequencies and they do not appear in the statistics of the coherence function. The coherence of the PRBS system exhibits large discrete sawtoothed band components with peaks and valleys of rapidly varying functional quality of the relationship between input and output. This results in a poor signal-to-noise ratio of the transfer function $H(f)$, as seen in Fig. 8. This figure indicates the degree of dynamic range superiority of the FT time delay spectrometer to that of the device operating with a PRBS excitation. The exceptional quality of the FM time delay spectrometer transfer function is intimately related to the quality of the impulse response, Fig. 3, whose Fourier transform the transfer function is. The magnitudes and phases calculated via FFT methods and displayed on the FFT analyzer screen are, in principle, the same curves obtained point-by-point in the dispersive frequency domain experiments of Part II using sinusoidal system excitation and lock-in detection. The importance of high-quality transfer function data lies in the fact that our FFT analysis can obtain the frequency response of the photothermal wave system under investigation within a minute fraction of the time required for the frequency domain measurement. In our case, for instance, the average transfer function acquisition time for a mean value over one thousand samples span-

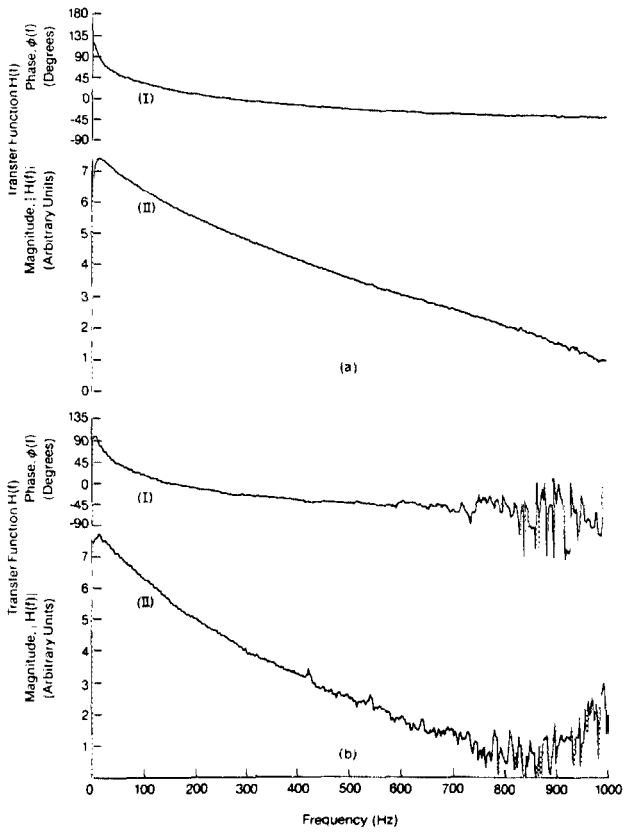

FIG. 8. Transfer function channels of the mirage effect system: (a) FT time delay spectrometer; (b) PRBS spectrometer. (I): phase; (II) magnitude.

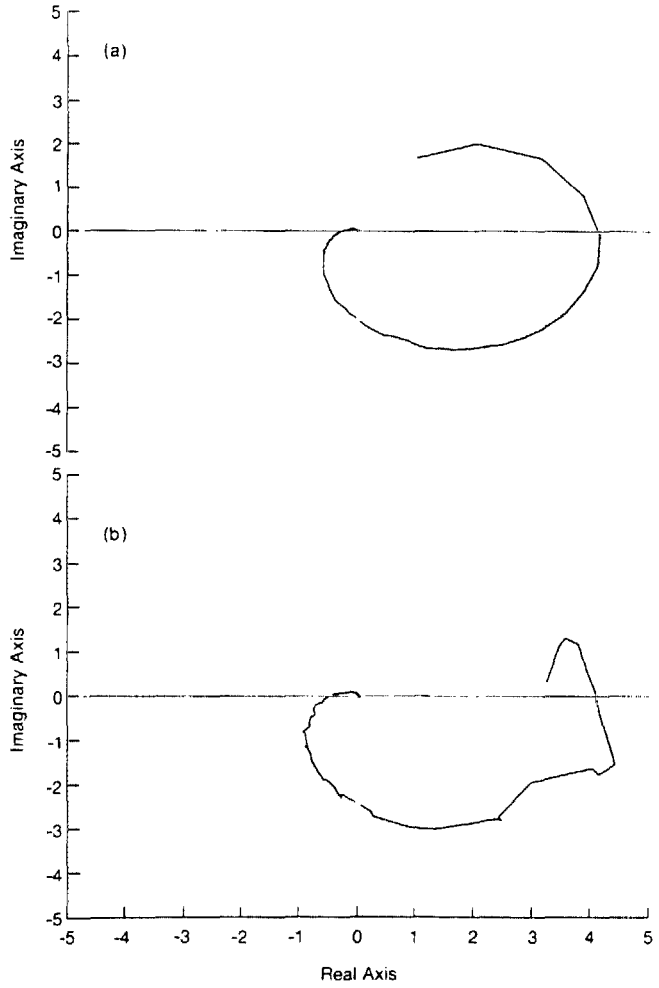

FIG. 9. Nyquist plots for (a) the FM time delay spectrometer, and (b) the PRBS spectrometer.

ning the entire frequency range of interest (dc to 1 kHz) at 1024 intervals was approximately 5 min. This is to be compared to $\sim\frac{1}{2}$ h required for scanning the same frequency range for a mean value over 20–40 samples at 20–30 intervals using lock-in detection. Figure 8 indicates a drop in the magnitude signal between approximately dc and 20 Hz and a phase distortion for both waveform types. This roll off is due to the combined actions of the preamplifier bandwidth high-pass limit set at 10 Hz and the spectral window (raised Hanning) superimposed on both waveforms. The frequency response observed at high frequencies is typical of photothermal deflection spectroscopic systems.[8,9] The very small ripple of the FM time delay spectrometer above 700 Hz shows excellent promise for high-quality photothermal imaging applications at high frequencies.

The frequency response plots of Fig. 8 can also be conveniently regarded as those of a low-pass filter from a systems engineering point of view, where the spectrometer is treated as a "black box." From this point of view it is then instructive to construct a Nyquist plot for the spectrometer as shown in Fig. 9. These plots are useful in describing the stability of the spectrometer regarded as a control system.[10] The simple loop responses shown in Fig. 9 are indicative of stable bounded systems with well-defined transient response in the time domain, however, the smoother, symmetrical with respect to the positive real axis Nyquist loop line for the FM time delay spectrometer is an indication of a higher degree of stability for this system than for the PRBS device.

ACKNOWLEDGMENTS

The authors wish to acknowledge the financial support of the Natural Sciences and Engineering Research Council of Canada (NSERC) throughout the work acomplished in all three parts of this report. They also wish to thank the Ministry of Transportation and Communications of the Province of Ontario for useful cooperation in the signal analysis of the FM time delay spectrometer apparatus.

[1] H. Coufal, J. Photoacoust. **1**, 413 (1983).
[2] Y. Sugitani, A. Uejima, and K. Kato, J. Photoacoust. **1**, 217 (1982).
[3] J. S. Bendat and A. G. Piersol, in *Engineering Applications of Correlation and Spectral Analysis* (Wiley, New York, 1980).
[4] H. M. Lai and K. Young, J. Acoust. Soc. Am. **72**, 2000 (1982).
[5] A. Rosencwaig, in *Photoacoustics and Photoacoustic Spectroscopy,* Chemical Analysis (Wiley, New York, 1980), Vol. 57.
[6] Y. Sugitani and A. Uejima, Bull. Chem. Soc. Jpn. **57**, 2023 (1984).
[7] K. R. Godfrey, Automation **16**, 527 (1980).
[8] W. B. Jackson, N. M. Amer, A. C. Boccara, and D. Fournier, Appl. Opt. **20**, 1333 (1981).
[9] J. C. Murphy and L. C. Aamodt, J. Appl. Phys. **51**, 4580 (1980).
[10] J. E. Alexander and J. M. Bailey, in *Systems Engineering Mathematics* (Prentice–Hall, Englewood Cliffs, NJ, 1962).